Sustainable Energy, Grids and Networks 28 (2021) 100537

Contents lists available at ScienceDirect

Sustainable Energy, Grids and Networks

journal homepage: www.elsevier.com/locate/segan

Impacts of grid-tied microgrid on stability and interaction of power systems considering RE uncertainties

Awan Uji Krismanto [a,b], N. Mithulananthan [b], Herlambang Setiadi [c,*], Eko Yohanes Setyawan [d], Muhammad Abdillah [e]

[a] Department of Electrical Engineering, National Institute of Technology, Malang, Indonesia
[b] School of ITEE, The University of Queensland, Brisbane, Australia
[c] Faculty of Advanced Technology and Multidiscipline, Universitas Airlangga, Surabaya, Indonesia
[d] Department of Mechanical Engineering, National Institute of Technology, Malang, Indonesia
[e] Department of Electrical Engineering, Universitas Pertamina, Jakarta, Indonesia

ARTICLE INFO

Article history:
Received 26 April 2021
Received in revised form 29 June 2021
Accepted 30 August 2021
Available online 1 September 2021

Keywords:
Microgrid
Uncertainties
Small signal stability
Interaction
Resonance
Modal interaction index

ABSTRACT

Increasing penetration of Renewable Energy (RE) based Microgrid (MG) introduces either beneficial or detrimental effects on power system stability. Uncertain condition of RE influences the dynamic behaviour of critical modes of power systems which potentially alter damping and increases the risk of oscillatory instability. On the other hand, it also reduces generator and transmission lines stress, enhancing the system stability. More complex MG control also leads to the occurrence of interaction among critical modes. More specific modal interaction in terms of resonance phenomenon potentially emerge when the engaged modes align both in damping and frequency of oscillation. In this paper, impacts of uncertain power injections from the RE based MG on small signal stability are thoroughly investigated using Monte Carlo (MC) simulation. From eigenvalues analysis, it was monitored that under RE uncertainties, the critical modes behaved randomly and unpredictably. However, the cumulative distributions of critical modes indicated that the additional power injections from the MG system introduced a positive impact in enhancing system stability. The presented work further discussed interaction among local, inter-area and control modes of MG due to variation of system parameters using a novel index known as Modal Interaction Index (MII). From several case studies, it is observed that MG contributed to mitigate resonance and modal interaction.

© 2021 Elsevier Ltd. All rights reserved.

1. Introduction

Distributed power generations (DG) have been extensively utilized due to its technical, economic and social benefits. However, since most of DG units are supplied by renewable energy (RE), the generated power is highly dependent on weather conditions. Therefore, stability and reliability issues have become major attentions in integrating RE based DG units into the existing grid. To manage with RE uncertainties and facilitate more integration of RE based DG units, it is advisable to combine several DG units into a single supervised and controlled power generation system. The combined system is popularly referred to as Microgrid (MG). Even though MG allows seamless integration of renewable power generations, increase MG penetration gradually transforms operation of the conventional power systems. Dominant features of the MG introduce novel challenges in system dynamic, protection scheme and load management [1]. Since most of the DG units in MG employed inertia-less power electronic as power conversion and interfacing devices, aggregated system inertia degrades proportionally. Reduction of system inertia may alter the system damping. Another concern in a grid-tied MG operation is random power injections from the MG due to uncertain RE sources. The RE uncertainties introduce unpredictable effects on critical low oscillatory modes of power system. Moreover, a sophisticated MG control also introduces non-linear effects on system dynamic behaviour and oscillatory circumstances which potentially lead to the occurrence of interactions between critical modes [2]. On the other hand, additional power injection from the MG system potentially reduces generator and transmission line stress and eventually enhance system stability.

Impact of grid-tied MG operation on small signal stability and modal interaction under RES uncertainties should be better understood as it brings various dynamic and non-linear behaviour of sensitive modes. Extensive researches have been carried out to assess impact of increasing RE penetration on oscillatory stability of power system. Initial research regarding influence of MG on low frequency oscillatory modes was presented in [3]. It has been

* Corresponding author.
E-mail address: h.setiadi@stmm.unair.ac.id (H. Setiadi).

https://doi.org/10.1016/j.segan.2021.100537
2352-4677/© 2021 Elsevier Ltd. All rights reserved.

reported that MG contributes to improve the damping condition of low frequency oscillation modes. In [4,5], investigation of large-scale Wind Energy Conversion System (WECS) effects on small signal stability have been presented. While, beneficial impacts of increasing wind power on system damping performance have been reported in [6,7]. It was clearly shown that high wind power penetration significantly enhanced damping ratio of low frequency modes of power system in particular inter-area modes. Improvement of local and inter-area modes of power system due to integration of PV and WECS was investigated in [8]. It was also monitored that impact of PV on small signal stability varies with the change of the operating condition [9,10].

Most of the previous studies corresponding to the oscillatory stability performance of power system with high RE penetrations considered a limited number of scenarios in a given range of power injections from the MG. Therefore, the obtained results did not reflect all the possible system dynamic behaviours. Moreover, the deterministic analysis might lead to under or over-estimated results depending on the selection of system parameters and operating conditions [11]. Therefore, an analytical approach which covers most possible power injection scenarios from MG is crucial in determining system stability boundaries and assessing risk of instability. To incorporate more scenarios corresponding to uncertain conditions of RE, a probabilistic approach was implemented. Monte Carlo (MC) and Quasi Monte Carlo (QMC) methods have been applied in [12,13], respectively to investigate impact of uncertain wind power injection on power system stability. While, in [14], a cumulant method is applied to enhance MC method in analysing the impact of large-scale wind power generation on oscillatory stability of power system. However, only simplified model of wind farm was considered in those researches, hence there is no contribution of wind power dynamic on power system stability. Moreover, the existing works did not investigate interaction between RE based power plant and critical modes of power system which potentially influence system stability. Interaction among sensitive modes possibly occurred when two or more eigenvalues have a proximity or an alignment in both damping and frequency [2,15,16]. Moreover, stressed operating circumstances of power system when it was operated under heavy loading condition, low system inertia, RE uncertainties and small disturbances increase the risk of modal interaction. Since the engaged modes become very sensitive to the parameter variations around the interaction point, more oscillatory situation was observed. Hence, modal interaction and resonance in power system might be an early indication for system instability.

This paper investigates the impacts of uncertain power injection from grid-tied hybrid MG operation on oscillatory stability of power system. Furthermore, possible interactions between sensitive eigenvalues is identified and confirmed through eigentrajectories, an index namely Modal Interaction Index (MII) [17] and participation factor analysis. Contributions of the paper can be highlighted as follows:

- Performing small signal stability analysis of power system involving dynamic models of hybrid MG system.
- Risk of instability analysis and stochastic assessment of damping ratio of critical modes.
- Influence of increasing penetration of MG on dynamic behaviour of critical modes and modal interactions.
- Identification the interaction events between weak modes of power systems and weak modes of MG.
- A novel index and cross participation factor analysis for identifying modal interaction and locate a resonance point.
- Case studies with realistic wind and solar irradiance profiles from four different regions.

The remainder of this paper is organized as follows. Proposed MG and its controllers are presented in Section 2. Section 3 describes probabilistic approach for analysing the dynamic behaviour of sensitive modes under uncertain power injection from MG. In Section 4, analytical procedure for investigating possible modal interaction is presented. The simulation results and discussion of increasing MG penetration effect on existing test systems are presented in Section 5. Eventually, conclusions and contributions of this paper are highlighted in Section 6.

2. Microgrid model

During grid-tied mode, each DG unit in MG is required to provide a pre-set power output for the main grid regardless of the load variations since most of the power demand can be handled by the grid. Therefore, these DG units do not contribute to power balancing and regulation of grid frequency and voltage [18]. Under normal condition of grid-tied operation, power inverter in each DG unit in MG is operated as a grid-feeding power converter in the constant current control mode [19–22]. The main control objective of the grid-feeding power converter is to maximize the power injection from each DG unit according to the actual RE conditions. Moreover, a robust synchronization among DG units within MG and the main grid is required to maintain stable operation of the power system with high penetration of RE power generations.

A typical block diagram of hierarchical control technique in a MG system under grid-connected operation is depicted in Fig. 1. Hierarchical control method is adopted as a compromise between fully centralized and decentralized control systems [23]. The proposed control method requires less communication and computational procedures than a fully centralized controller. Moreover, it provides a sufficient synchronization control signal which cannot be offered by the fully decentralized control method. Three control layers; primary, secondary and tertiary controllers are considered in the hierarchical control. The primary control which is the first layer of the MG control is responsible for controlling the local variables such as local voltage, frequency and power output of each DG unit. However, in grid-tied mode, each DG unit in MG is controlled to extract the maximum available RES power while frequency and voltage regulations are handled by the main grid. The secondary control level in MG system is in charge of compensating voltage and frequency deviation and restoring the frequency and voltage values to their nominal values. Moreover, the second control layer is responsible for providing the coordination control signal for synchronization and dispatching purposes of each DG units [18]. Finally, the third control layer corresponding to tertiary control level is responsible for coordinating the optimal operation and power management among MG systems and the main grid [23,24]. Since only one MG system is considered in this research, only primary and secondary control layers of the MG system are considered.

A hybrid MG system can be defined as a MG system which consists of combination of DG units powered by various RES. Specifically, in this paper, the hybrid MG system consisting of WECS and PV based DG units is considered. Regulation of active and reactive power from MG is realized by local control systems of each DG unit which are shown in Fig. 2. The synchronization controller based on a phase lock loop (PLL) is applied to determine the angle, frequency and voltage references for each DG unit. Transformation of the measured grid voltage into a rotating reference frame domain is applied to obtain direct and quadrature axis of grid voltage (v_{dgrid}, v_{qgrid}). The v_{qgrid} is regulated by PI controller to determine the reference values of angular frequency (ω_{ref}). A reference phase angle (δ_{ref}) for the corresponding DG unit is then determined from integral operation of ω_{ref}. Moreover,

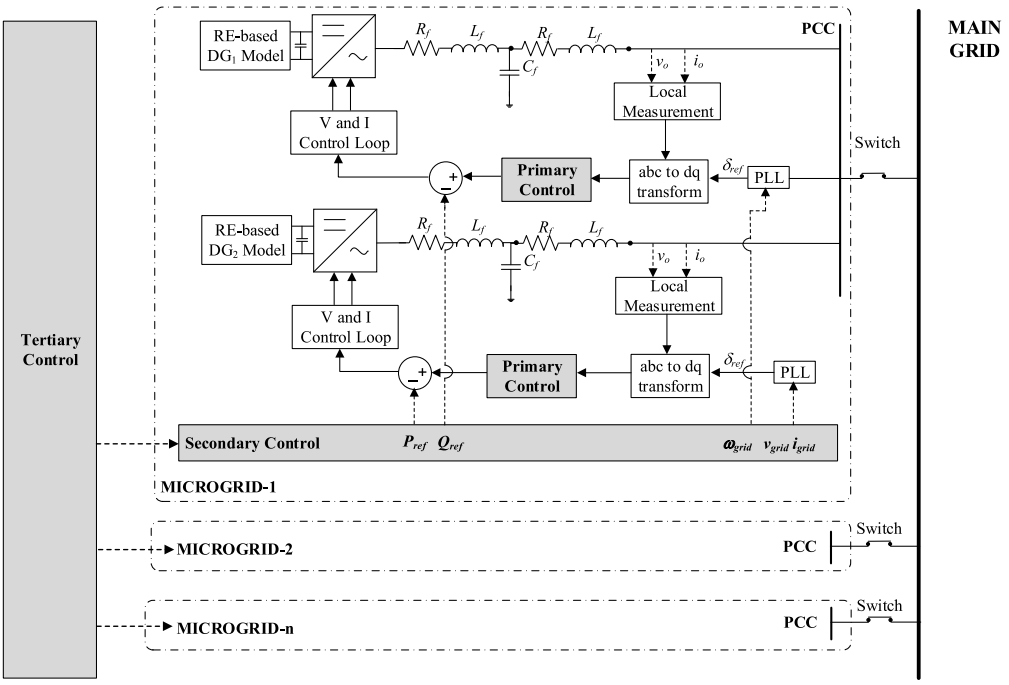

Fig. 1. Investigated hybrid microgrid system.

reactive power reference (Q_{ref}) is obtained from the regulation of the difference between $v_{dgrid}v_{dgrid}$ and reference voltage values $(v_{dref})(v_{dref})$.

The synchronization controller based on a phase lock loop (PLL) is applied to determine the angle, frequency and voltage references to ensure stiff synchronized operation with the grid. The measured grid voltage is transformed into a rotating reference frame domain to obtain direct and quadrature axis of grid voltage (v_{dgrid}, v_{qgrid}). The v_{qgrid} is then regulated by PI controller to determine the reference values of angular frequency (ω_{ref}). A reference phase angle (δ_{ref}) for the corresponding DG unit is then determined from integral operation of the angular frequency. Moreover, reactive power reference is obtained from the regulation of the difference between v_{dgrid} and reference voltage values (v_{dref}). The state equation of PLL controller is derived using the auxiliary variables state variables $(\varphi_{dPLL}, \varphi_{qPLL})$ as follows:

$$\frac{d\varphi_{dPLL}}{dt} = v_{dref} - v_{dgrid}, \frac{d\varphi_{qPLL}}{dt} = v_{qref} - v_{qgrid} \quad (1)$$

The algebraic equations of reference reactive power and angular frequency are given by equation (2) and (3) respectively:

$$Q_{ref} = K_{iPLL}\varphi_{dPLL} + K_{pPLL}\left(v_{dref} - v_{dgrid}\right) \quad (2)$$

$$\omega_{ref} = K_{iPLL}\varphi_{qPLL} + K_p\left(v_{qref} - v_{qgrid}\right) \quad (3)$$

The following sections present descriptions of local controller of each RE based DG unit in the investigated MG system.

2.1. WECS based DG unit control system

In this research, a fully rated converter type of wind generator with back-to-back converter and DC link is employed. The beneficial features of the back to back converter is the fast control of power flow hence it can deal with the variation of wind speed. As shown in Fig. 2, control system in the selected WECS consisting of generator and grid side converter control. The generator side converter is responsible for maintaining the terminal voltage and frequency of the generator according to optimal rotational speed of the wind turbine. While, the DC link between two converter behaves as an energy storage device to maintain stable power output from generator side converter.

The generator side AC/DC converter incorporates outer and inner control loops. The outer control loop measured terminal generator and DC link voltage and compared those measured voltages to their reference values. The determined errors are then controlled using conventional PI control method to derive reference values of direct and quadrature currents. By considering β_{dgen} and β_{qgen} as auxiliary state variables of outer control loop of generator side converter, state equations of the controller can be stated as

$$\frac{d\beta_{dgen}}{dt} = v_{dcref} - v_{dc}, \frac{d\beta_{qgen}}{dt} = v_{gen\_ref} - v_{gen} \quad (4)$$

The equations of reference current of generator side converter are given by the following equations

$$i_{dgen\_ref} = K_{i21}\beta_{dgen} + K_{p21}v_{dcref} - K_{p21}v_{dc} \quad (5)$$

$$i_{qgen\_ref} = K_{i11}\beta_{qgen} + K_{p11}v_{gen\_ref} - K_{p11}v_{gen} \quad (6)$$

Output variables from the outer control loop are then applied to inner current control loop as reference values and compared to the actual values of generator currents (i_{dgen}, i_{qgen}). Auxiliary state variables of γ_{dgen} and γ_{qgen} are required to provide state equation of the inner current controller as given by

$$\frac{d\gamma_{dgen}}{dt} = i_{dgen\_ref} - i_{dgen}, \frac{d\gamma_{qgen}}{dt} = i_{qgen\_ref} - i_{qgen} \quad (7)$$

A similar algorithm is implemented to the current control loop to determine the modulation indices (m^*_{dgen}, m^*_{qgen}) for the generator-side converter. These modulation indices are afterward employed as control variables of PWM switching scheme for the converter. The algebraic equations of modulation indices reference signal for generator side converter are given by the following equations:

$$m^*_{dgen} = K_{i41}\gamma_{dgen} + K_{p41}i_{dgen\_ref} - K_{p41}i_{dgen} \quad (8)$$

$$m^*_{qgen} = K_{i31}\gamma_{qgen} + K_{p31}i_{qgen\_ref} - K_{p31}i_{qgen} \quad (9)$$

Similar to the generator-side control, the grid-side inverter control in fully rated WECS based DG units is consisting of outer

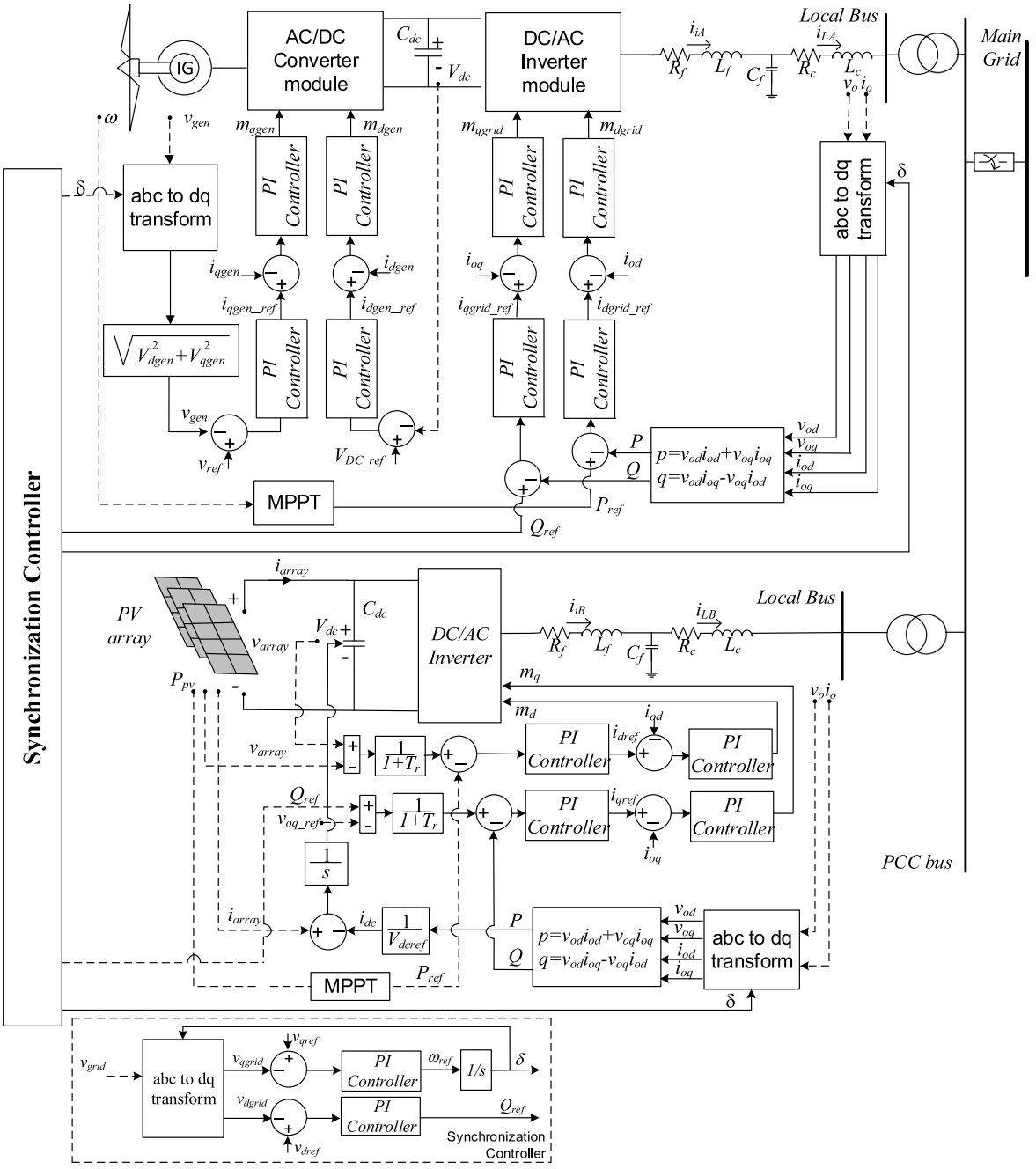

Fig. 2. Control system of each DG nit in the investigated MG system.

and inner control loops. In the outer control loop, the calculated active and reactive power reference values are compared to the measured active and reactive output power of the DG unit. State equation of grid side outer control loop can be derived by considering β_{dgrid} and β_{qgrid} as auxiliary state variables using the following equations

$$\frac{d\beta_{dgrid}}{dt} = P_{ref} - P, \frac{d\beta_{qgrid}}{dt} = Q_{ref} - Q \tag{10}$$

The obtained error from outer control loop is then regulated by PI controller, yielding the reference values for the inner current control loop as follows

$$i_{dgrid\_ref} = K_{i22}\beta_{dgrid} + K_{p22}P_{ref} - K_{p22}P \tag{11}$$

$$i_{qgrid\_ref} = K_{i12}\beta_{qgrid} + K_{p12}Q_{ref} - K_{p12}Q \tag{12}$$

Moreover, the inner current controller loop generated modulation indices $\left(m^*_{dgrid}, m^*_{qgrid}\right)$ for providing switching signal for grid side inverter. Auxiliary state variables of γ_{dgrid} and γ_{qgrid} are required to provide state equations of the inner current controller loop as given by

$$\frac{d\gamma_{dgrid}}{dt} = i_{dgrid\_ref} - i_{od}, \frac{d\gamma_{qgrid}}{dt} = i_{qgrid\_ref} - i_{oq} \tag{13}$$

The algebraic equations of modulation indices reference signal for grid-side inverter are given by

$$m^*_{qgrid} = K_{i32}\gamma_{qgrid} + K_{p32}i_{qgrid\_ref} - K_{p32}i_{oq} \tag{14}$$

$$m^*_{dgrid} = K_{i42}\gamma_{dgrid} + K_{p42}i_{dgrid\_ref} - K_{p42}i_{od} \tag{15}$$

2.2. PV based DG unit control system

The dynamic model of PV based DG unit is consisting of a dynamic model of PV array, DC-link and DC/AC power inverter. Conventional control of PV system incorporates Maximum Power Point Tracking (MPPT) control algorithm to ensure maximum power extraction from available solar power. Since, response of MPPT controller in PV system is much slower than inverter controller, it can be assumed that for small variation of solar irradiance and temperature, PV array voltage is constant.

Interface between PV system and existing grid is facilitated by a DC/AC inverter. Similar to WECS based DG unit, control algorithm of grid side inverter in the PV based DG unit is consisting of outer and inner control loops. It is assumed that the corresponding PV system is operated at its maximum power point (MPP). Active power reference (P_{ref}) is obtained from the MPP active power. The calculated reference value is then compared with the difference between measured DC link voltage and actual voltage at the MPP. Reactive power reference (Q_{ref}) is calculated based on the difference between terminal PV system and reference voltages. By considering ρ_{dPV} and ρ_{qPV} as auxiliary state variables of outer control loop of grid-side inverter, state equations of the controller can be stated as in.

$$\frac{d\rho_{dPV}}{dt} = \left(V_{dc} - V_{pv}\right) - P_{ref}, \frac{d\rho_{qPV}}{dt} = \left(v_{oq} - v_{ref}\right) - Q \tag{16}$$

The obtained error is regulated by PI controller to establish d-axis current reference value using the following equations

$$i_{dPV\_ref} = K_{iPV1}\rho_{dgrid} + K_{pPV1}\left(V_{dc} - V_{pv}\right) - K_{pPV1}P_{ref} \tag{17}$$

$$i_{qPV\_ref} = K_{iPV2}\rho_{qgrid} + K_{pPV2}\left(v_{oq} - v_{ref}\right) - K_{pPV2}Q \tag{18}$$

The obtained reference currents are then subsequently fed to the inner current control loop and compared to the measured output current of PV system. Eventually, the calculated error is regulated by PI to generate control signals $\left(m^*_{dPV}, m^*_{qPV}\right)$ for the grid-side inverter of the PV system. These modulation indices are afterward employed as control variables of PWM switching scheme for the inverter. Auxiliary state variables are required to provide state equations of the current controller loop as given by

$$\frac{d\varphi_{dPV}}{dt} = i_{dPV\_ref} - i_{od}, \frac{d\gamma_{qPV}}{dt} = i_{qPV\_ref} - i_{oq} \tag{19}$$

The algebraic equations of modulation indices reference signal for grid-side inverter in PV system are given by

$$m^*_{dPV} = K_{iPV3}\varphi_{dPV} + K_{pPV3}i_{dPV\_ref} - K_{pPV3}i_{od} \tag{20}$$

$$m^*_{qPV} = K_{iPV4}\varphi_{qPV} + K_{pPV4}i_{qPV\_ref} - K_{qPV4}i_{oq} \tag{21}$$

3. Probabilistic small signal stability

Probabilistic approach in small signal stability analysis aims to estimate the distribution and assess the risk of instability of critical eigenvalues under RE uncertainties. Uncertain RE conditions were determined from the probabilistic distribution function (*pdf*) of wind speed and solar irradiance. In this paper, hybrid MG structure which consisting of WECS and PV based DG units was considered to investigate the impacts of RE uncertainties on the oscillatory stability of a power system.

Power output of PV based DG units varied as a function of solar irradiance and PV cell temperature. The proposed PV array model for the stability study is presented in [25]. According to PV cell characteristics, the photocurrent is proportionally correlated to solar irradiance variation. While the terminal voltage of PV array is inversely proportional to the temperature [26]. It was observed that solar irradiance variation affects the PV cell temperature. However, since the temperature change is much slower than the sudden change of irradiance, it can be neglected in evaluating the dynamic behaviour of the PV array [25,27]. To simplify the analysis, it can be considered that the terminal voltage of a PV array is constant at the optimum operating point. Therefore, the output power from PV based DG units varied in proportion with a variation of solar irradiance [28]. The correlation between output power of a PV system and solar irradiance is depicted in Fig. 3 [29].

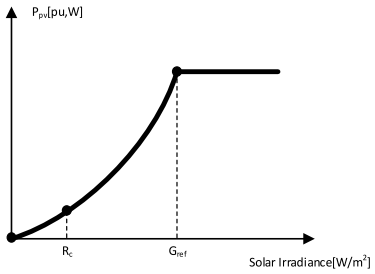

Fig. 3. PV power curve.

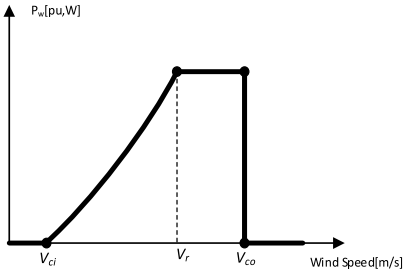

Fig. 4. Wind power curve.

The typical power output from a PV system can be expressed as a function of solar irradiance using (22) [30].

$$P_{pv}(G_t) = \begin{cases} P_{rpv}\dfrac{G_t^2}{G_{std}R} & for \quad 0 < G_t < R_c \\ P_{rpv}\dfrac{G_t}{G_{std}} & for \quad R_c < G_t < G_{std} \end{cases} \tag{22}$$

Where P_{pv} and P_{rpv} represent power outputs at a particular solar irradiance and equivalent rated power outputs of PV system respectively. R_c indicates a certain radiation point set as 150 W/m^2, While G_t and G_{std} represent actual and standard values (1000 W/m^2) of solar irradiance respectively. In this research, it is considered that the rated power output of PV based DG unit is 50 MW at the rated solar irradiance value of 1000 W/m^2.

Wind power from WECS based DG units is highly correlated to the mechanical characteristic of the wind turbine, power output curve and actual values of wind speed. The typical power curve for a wind generator is depicted in Fig. 4. In general, the operating point of the wind turbine is starting with a particular wind speed, namely cut-in wind speed (V_{ci}). At lower than V_{ci}, the wind turbine is not operated due to efficiency reasons. The generated wind power increase proportionally as the actual wind speed increase in the range of cut-in wind speed (V_{ci}) to rated wind speed (V_r). As the wind speed continuously vary from rated wind speed (V_r) to cut-off wind speed (V_{co}), the power output from the wind turbine is maintained at the rated power level. However, beyond the cut-off speed, the corresponding wind turbine would be shut down for safety considerations [31].

According to the presented power curve, the power output of a WECS can be calculated as a function of actual wind speed

by applying a simplified input–output function as given by (23) [32,32,33].

$$P_w(v_w) = \begin{cases} 0 & for \quad v < v_{ci} \ or \ v > v_{co} \\ \dfrac{v_w - v_{ci}}{v_r - v_{ci}} P_{wr} & for \quad v_{ci} \le v \le v_r \\ P_{wr} & for \quad v_r < v < v_{co} \end{cases} \tag{23}$$

Where P_w and P_{wr} represent a power output at a particular wind speed and the equivalent rated power output of WECS respectively. In this research, the WECS based DG unit has a rated capacity of 50 MW, and the power output from these RES base DG units varies as a function of V_{ci}, V_r and V_{co} which have values of 3 m/s, 12.5 m/s and 25 m/s respectively.

Small signal models of PV and WECS based DG units as presented in previous section were integrated to form the hybrid MG structures. Active power dispatch levels and stochastic distributions of power injections from RE based DG units within MG were calculated according to the estimated *pdf* of wind speed and solar irradiance using (1) and (2) respectively. System eigenvalues are calculated using modal analysis method. The Modal analysis which describes the dynamic behaviour of the system when it is exposed to then small disturbances, is derived from the linearization of non-linear system dynamic equations around a certain operating point. Dynamic responses and oscillatory stability of power systems were then evaluated by investigating the probabilistic distribution of local and inter-area electro-mechanical modes. The *pdfs* of those critical modes were determined by randomly sampled the uncertain generated power from the investigated MG system through an iterative method such as Monte Carlo (MC) simulation. Moreover, variation of critical modes damping ratio would be observed to assess the risk of unstable situations.

The MC simulation is applied in probabilistic small signal stability study to investigate the random behaviours of the critical eigenvalues when the system is subjected to an uncertain condition on system parameters or a small disturbance. The main procedure of probabilistic small signal stability analysis is presented in Fig. 5 [34]. Random power generations from RE based DG units were generated. The dynamic behaviour of local and inter-area modes of power system under uncertain power injection were then evaluated iteratively using modal analysis method. From the obtained eigenvalues, the clustering technique is applied to extract the investigated modes. Eventually, the system damping and dynamic responses are assessed statistically to determine the risk of instability and small signals stability performance.

4. Modal interactions

Analytical procedure of small signal stability can be conducted through linearization of equations associated to system dynamic response as given by the following state equation

$$\Delta\dot{x} = A\Delta x + B\Delta u \tag{24}$$

Where A and B respectively represent system state and input matrices. While state and input variables matrices are given by Δx and Δu respectively.

The eigenvalues of matrix A are presented by scalar values of λ which satisfies the non-trivial solution to the following equation

$$A\phi = \lambda\phi \tag{25}$$

The n-column vector of ϕ_i is defined as right-eigenvector of A correspond to a specific eigenvalue of λ_i. Where, n is the number of state variables. The right eigenvector for a particular mode has the form of

$$\phi_i = \begin{bmatrix} \phi_{1i} & \phi_{2i} & \cdots & \phi_{ni} \end{bmatrix}^T$$

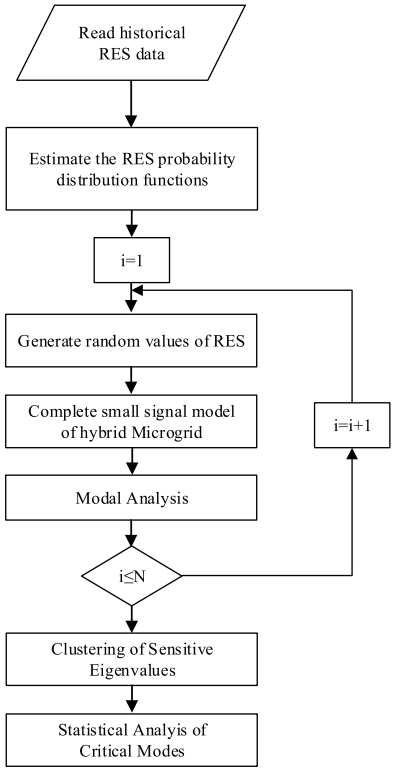

Fig. 5. MC simulation for probability small signal stability analysis [34].

Similarly, n-row vector of ψ_i which satisfied the equation of

$$\psi A = \lambda\psi \tag{26}$$

is defined as left-eigenvector for a specific eigenvalue of λ_i. The associated left-eigenvector is given by this following form

$$\psi_i = \begin{bmatrix} \psi_{1i} & \psi_{2i} & \cdots & \psi_{ri} \end{bmatrix}$$

The left and right-eigenvectors corresponding to two different eigenvalues ($\lambda_i \neq \lambda_j$) are orthogonal [35]. Hence product of left and right-eigenvector for different modes is given by

$$\psi_i\phi_j = 0 \tag{27}$$

While, for similar eigenvalues ($\lambda_i = \lambda_j$), the non-zero constant product of left and right eigenvector is obtained as

$$\psi_i\phi_j = C_{ij} \tag{28}$$

Activities of state variables which are represented by left and right eigenvectors can be considered as an indicator of the occurrence of modal interaction [35,36]. Even though both eigenvalues come from different parts of the system, the mode coupling might arise due to similarity of eigenvectors [37]. When some modes situated closely, they potentially interact and resonate in a particular point. Around a resonance point, the engaged modes are highly sensitive to parameter variations. Trajectories of involved modes departure quickly and deviate significantly. One of these modes possibly moves at right angle, result in deterioration of system small signal stability. Even, strong resonance in power system potentially cause the system instability [16].

When a coupling among eigenvalues occurs, dynamic response of a particular state variable from one mode might also exhibit in other modes and influences the trajectories and damping performance of the interacting modes. Connection or coupling between two eigenvalues might be identified from the product of right and left eigenvectors. When the two modes are completely

decoupled, the product of their right and left eigenvectors will be zero. On the other hand, if there is a coupling between two eigenvalues, the non-zero values of left and right eigenvector products is identified. Therefore, degree of modal interaction can be measured by cross product of right and left eigenvectors of the interacting modes. To quantify the occurrence of interaction, a Modal Interaction Index (MII) as proposed in [17] is applied. The MII between two interacting eigenvalues of λ_i and λ_j when kth state variable is contributing in both of the coupling modes is given by

$$MII = \phi_{ik}\psi_{kj} + \phi_{jk}\psi_{ki} \tag{29}$$

Through this relationship, it is observed that higher values of MII indicated occurrence of stronger modal interaction. It is possible that more than one state variables are participating in both interacting modes. Therefore, the measured index needs to be expanded when more than one state variable contributing in both of interacting modes. When n state variables are participating in those two λ_i and λ_j eigenvalues, the MII can be presented as given by

$$MII = \left(\phi_{i1}\psi_{1j} + \phi_{j1}\psi_{1i}\right) + \left(\phi_{i2}\psi_{2j} + \phi_{j2}\psi_{2i}\right) + \cdots + \left(\phi_{in}\psi_{nj} + \phi_{jn}\psi_{ni}\right) \tag{30}$$

In general form, the MII can be stated as

$$MII = \sum_{k=1}^{n}\left(\phi_{ik}\psi_{kj} + \phi_{jk}\psi_{ki}\right) \tag{31}$$

The interaction and resonance among neighbouring eigenvalues can also be confirmed by observing contribution of state variables in the coupling modes [38]. Interaction between two modes is expected when at least one state variables from each mode participate in both of the engaged eigenvalues. Let participation factor of ith state variables and the kth modes is denoted by p_{ik} and defined as

$$p_{ik} = \phi_{ik}\psi_{ik} \tag{32}$$

Where ϕ_{ik} and ψ_{ik} respectively represent the element on the right eigenvector and left eigenvector.

5. Results and discussions

In this paper, two area power system as shown in Fig. 6 is considered as a test bed system. Each area has 2 synchronous generators; G1, G2 in area 1 and G3, G4 in area 2. All generator are equipped with exciter and governor system. Dynamic parameters of synchronous generators are adopted from [35]. Total load of areas 1 and 2 are 967 MW and 1767 MW, respectively. In base case scenario without MG, 400 MW is delivered from Area 1 to supply load demand in Area 2. Some modifications were considered. Inertia constant of generator G1 and G4 were reduced to 2.6 and 4, respectively. Furthermore, some portion of generated power from G1 was decreased to 400 MW and transferred to G2 to realize more stressed condition in G2.

5.1. Impacts of uncertain power injection from MG on small signal stability

More stability challenges might emerge when power system is subjected to various types of RE uncertainties. Combinations of wind speed (WR1–WR4) and solar irradiance (SR1–SR4) *pdfs* from four different areas as presented [34] were considered. The statistical characteristics of wind speed and solar irradiance are presented in Table 1. It was clearly shown that region 4 has the highest RE profiles as represented by the highest values of mean and standard deviations of wind and solar irradiance respectively.

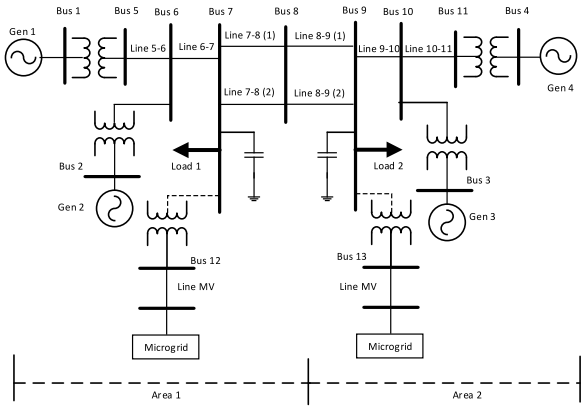

Fig. 6. Two area power system with penetration of hybrid MG.

Table 1
Statistical characteristics of wind speed and solar irradiance.

Wind regime	Mean	Standard deviation	Solar regime	Mean	Standard deviation
WR1	5.414	3.007	SR1	746.928	192.478
WR2	5.803	3.087	SR2	648.896	182.973
WR3	5.502	3.250	SR3	803.424	231.486
WR4	7.599	4.966	SR4	886.745	219.423

The proposed hybrid MG model was integrated to load bus in area-1 and area-2 to investigate the possible impacts of uncertain power injection from RE based power generation on oscillatory stability of power system and modal interactions. Generated power of WECS and PV based DG units within the investigated MG structure was varied in accordance with the *pdfs* of wind speed and solar irradiance profiles using (1) and (2) respectively. Moreover, to realize uncertain power injection from hybrid MG, the 10000 values of generated active power from each DG unit were then randomly sampled through MC simulation.

From eigenvalues analysis, it was observed that the electromechanical modes of two area power system is consisting of two local and one inter-area modes. The local modes 1 is corresponding to rotor angle (δ_1, δ_2) and speed (ω_1, ω_2) of G1 and G2. While local modes 2 is relating to rotor angle (δ_3, δ_4) and speed (ω_3, ω_4) of G3 and G4. The inter-area mode corresponds to rotor angle and speed of G1 to G4. It was also monitored that inter-area mode is more critical than local modes as indicated by lower damping ratio values of inter-area mode than local modes. Hence the inter-area mode potentially causes system instability when small perturbation occurred.

Trajectory plots of the local and inter-area modes when the hybrid MG system was integrated in area-1 are depicted in Figs. 7 and 8 respectively. From the presented eigen-trajectories, it was observed that with two sources of uncertainties were considered, the local and inter-area modes behaved unpredictably. More scattered positions of the critical modes were observed. However, even though more distributed eigen-positions were monitored, both of the investigated modes were situated in the left-hand side of the complex plane. These indicated that system stability can be maintained during wind speed and solar irradiance fluctuations.

Statistical analysis of local and inter-area modes of the two-area power system affected by uncertain power injection from hybrid MG in area-1 is presented in Table 2. The obtained results monitored that the stochastic distributions of inter-area mode considering RES uncertainties in regions 1, 2 and 3 were relatively similar. However, at a higher power injection level from MG which corresponds to higher wind speed and solar irradiance profiles as given in region 4, dynamic response of the critical

Table 2
Statistical analysis of critical modes of two-area power system under hybrid MG active power uncertainty in area 1.

Reg.	Local mode area 1						Local mode area 2						Inter-area mode					
	Re.		Im.		Damp. (%)		Re.		Im.		Damp. (%)		Re.		Im.		Damp. (%)	
	Mean	Std.	Mean	Std.	Mean	Std.	Mean	Std.	Mean	Std.	Mean	Std.	Mean	Std.	Mean	Std.	Mean	Std.
WR1-SR1	−0.805	0.011	9.375	0.010	8.56	0.001	−0.834	0.001	9.557	0.002	8.70	0.0001	−0.048	0.001	3.756	0.01	1.29	0.0001
WR2-SR2	−0.811	0.013	9.378	0.011	8.62	0.001	−0.835	0.001	9.558	0.003	8.69	0.0001	−0.049	0.001	3.758	0.01	1.30	0.0001
WR3-SR3	−0.809	0.012	9.376	0.010	8.59	0.001	−0.835	0.001	9.557	0.003	8.70	0.0001	−0.049	0.001	3.757	0.01	1.30	0.0002
WR4-SR4	−0.824	0.017	9.389	0.017	8.74	0.002	−0.836	0.001	9.561	0.005	8.71	0.0002	0.049	0.001	3.766	0.02	1.30	0.0003

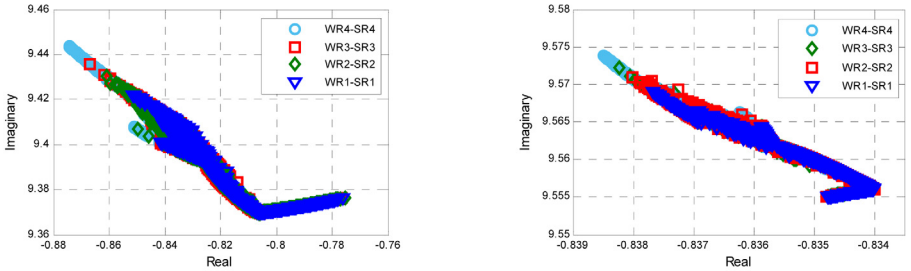

Fig. 7. Trajectories of (a) local mode-1and (b) local mode 2 under hybrid MG active power uncertainty in area-1.

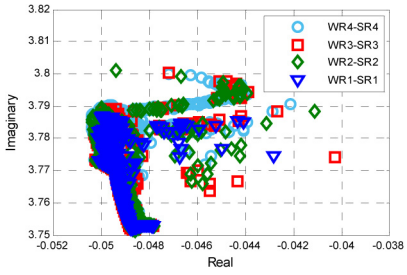

Fig. 8. Trajectories of inter area mode under hybrid MG active power uncertainty in area-1.

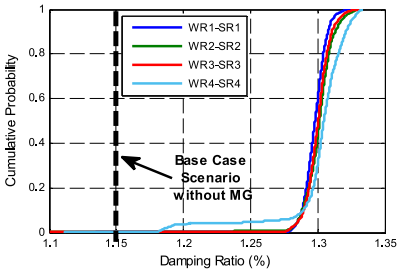

Fig. 10. CDF curve of inter-area mode damping ratio from two-area power system under hybrid MG power uncertainty in area 1.

modes slightly improved, indicated by a higher damping ratio. At higher wind speed and solar irradiance profiles as given in region 4 (WR4–SR4), the mean values of local mode 1, local mode 2, and inter-area modes damping ratio increased to 8.74%, 8.75% and 1.30% respectively.

The *CDF* of local and inter-area modes damping ratio when hybrid MG was connected to area-1 is depicted in Figs. 9 and 10 respectively. System stability enhancements were observed under grid-tied operation of MG. In base case scenario, the damping ratio of local modes 1, 2 and inter-area mode were 8.15%, 8.65% and 1.15% respectively. As power injection from the MG increased, the damping ratio of local modes 1, 2 and inter-area mode enhanced variously in the ranges of 8.2% to 9.2%, 8.695% to 8.73% and 1.1% to 1.35% respectively. The cumulative distribution of damping ratio of local mode 1 and local mode 2 enhanced proportionally with the increase of wind speed and solar irradiance profiles in regions 1, 2, 3 and 4. Similarly, the cumulative distribution of damping ratio of inter-area modes slightly increased in proportion with the increase of RE profiles.

In second case study, the hybrid MG was connected to load bus in area-2. Trajectories of local and inter-area modes when the hybrid MG was connected to area 2 are shown in Figs. 11 and 12 respectively. From the obtained eigen-trajectories, it was clearly observed that local mode 1 extensively moved to the left-hand side in proportion with the random increase of wind speed and solar irradiance, indicating an enhancement of system oscillatory stability. On the other hand, local mode 2 departed oppositely toward the imaginary axis, indicating a degradation

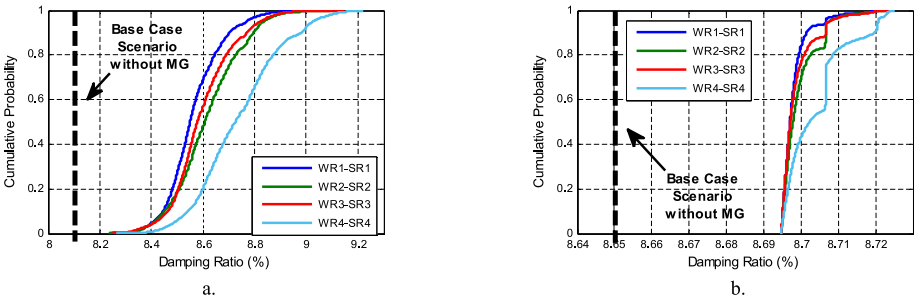

Fig. 9. CDF curve of damping ratio of local mode 1(a) and local mode 2(b) from two-area power system under hybrid MG power uncertainty in area 1.

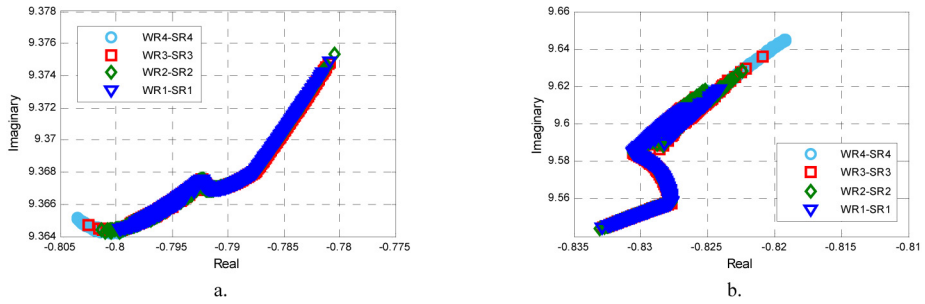

Fig. 11. Trajectories of (a) local mode-1and (b) local mode 2 under hybrid MG active power uncertainty in area-2.

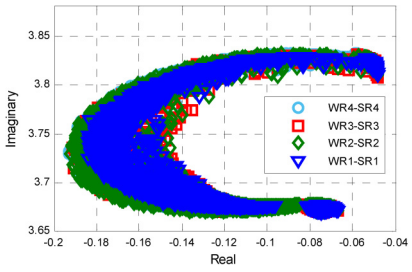

Fig. 12. Trajectories of inter area mode under hybrid MG active power uncertainty in area-2.

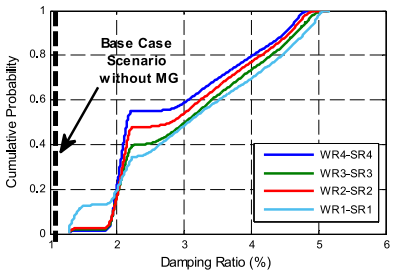

Fig. 14. CDF curve of damping ratio of inter-area mode from two-area power system under hybrid MG power uncertainty in area 2.

of system damping. More scattered and distributed positions of inter-area mode were observed. Primarily, the inter-area modes departed toward the left-hand side of the complex plane. As RES was; fluctuating more, those critical modes departed oppositely, resulting in degradation of system dynamic response.

The statistical analysis of local and inter-area modes of the two-area power system affected by uncertain power injection from the hybrid MG in area 2 is presented in Table 3. From the presented results, it was suggested that less damped circumstances occurred when the power injections from the investigated MG system were derived from the region with lower wind speed and solar irradiance profiles. The lowest mean values of real part, imaginary part and damping ratio of local mode 1 and inter-area modes were observed when the hybrid MG was operated in region 1 which had the lowest RE profiles. The dynamic performance of local mode 2 with the RE profiles from region 1 was relatively similar with that in regions 2 and 3. A significant increase of damping ratio of local mode 1 and inter-area modes were monitored in region 4 which had the highest RE profiles. Only a small decrease of damping ratio of local mode 2 was observed in those regions. Therefore, it can be considered that higher power injection from MG result in more enhancement of system small signal stability.

Cumulative distributions of damping ratio of local and inter-area modes with the presence of MG in area 2 are depicted in Figs. 13 and 14 respectively. Wind speed and solar irradiance variations associated with the uncertain MG power injection levels in area 2 brought different impacts on dynamic behaviours of the critical modes. As depicted in Fig. 13a, cumulative distribution of damping ratio of local mode 1 enhanced moderately when uncertain power injection from the hybrid MG in area 2 was considered. In base case scenario, the damping ratio of local mode 1 was 8.15%. As the hybrid MG was connected to area 2, the damping ratio of the corresponding modes enhanced moderately from 8.3% to 8.55% with the increase of RE profiles. On the contrary, uncertain power injection from the MG system deteriorated stability performance of local mode 2. As depicted in Fig. 13b, in the base case scenario, the damping ratio of local mode 2 was 8.65%. As power injection from MG varied in proportion with wind and solar irradiance values, the damping ratio of local mode 2 gradually decreased from 8.65% to 8.45% with the increase of RE profiles. Interestingly, it can be seen in Fig. 14 that uncertain power injection from the MG system in area 2 significantly improved damping performance of inter-area mode. Without additional power from the MG, damping ratio of the inter-area mode was 1.15%. However, with the random power injection from MG, the damping ratio of inter-area mode increased remarkably from 1.25% to 5.5% with the increase of wind speed and solar irradiance profiles. The inter-area mode

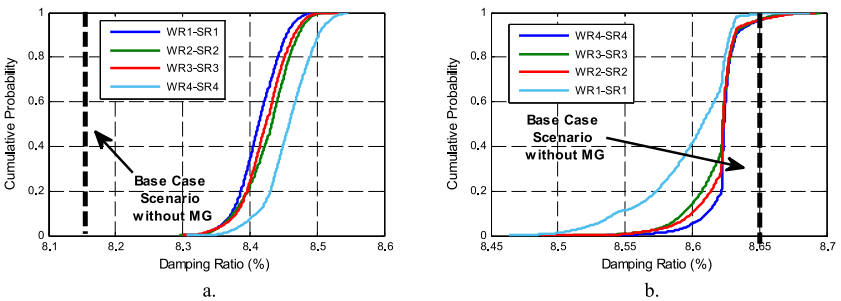

Fig. 13. CDF curve of damping ratio of local mode 1(a) and 2(b) from two-area power system under hybrid MG power uncertainty in area 2.

Table 3
Statistical analysis of critical modes of two-area power system under hybrid MG active power uncertainty in area 2.

Reg.	Local mode area 1						Local mode area 2						Inter-area mode					
	Re.		Im.		Damp. (%)		Re.		Im.		Damp. (%)		Re.		Im.		Damp. (%)	
	Mean	Std.	Mean	Std.	Mean	Std.	Mean	Std.	Mean	Std.	Mean	Std.	Mean	Std.	Mean	Std.	Mean	Std.
WR1-SR1	−0.791	0.003	9.367	0.001	8.41	0.001	−0.823	0.001	9.575	0.014	8.62	0.0002	−0.105	0.038	3.693	0.037	2.86	0.012
WR2-SR2	−0.792	0.003	9.367	0.001	8.42	0.001	−0.828	0.001	9.581	0.016	8.62	0.0002	−0.115	0.040	3.698	0.041	3.11	0.011
WR3-SR3	−0.792	0.004	9.367	0.002	8.42	0.001	−0.829	0.001	9.579	0.015	8.62	0.0002	−0.110	0.039	3.697	0.043	2.97	0.010
WR4-SR4	−0.795	0.004	9.366	0.001	8.46	0.001	−0.828	0.002	9.595	0.016	8.60	0.0003	−0.117	0.045	3.724	0.064	3.14	0.119

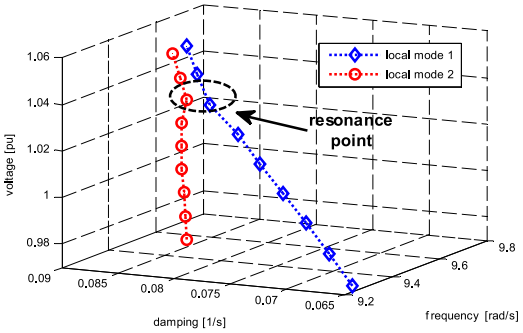

Fig. 15. Trajectories of local modes under variation of slack generator reference voltage.

had much lower damping ratio than local modes 1 and 2. Consequently, a significant increase of the damping ratio of inter-area modes provides a greater beneficial impact in enhancing the overall system small signal stability performance.

5.2. Impacts of MG penetration on interaction between local modes of power system

The proximity and similarities of oscillatory frequency of local modes potentially lead to the occurrence of modal interaction even though those sensitive modes are not electronically connected. It was monitored that the interaction between local modes from areas 1 and 2 potentially emerged under variation of slack generator voltage reference value. To investigate the dynamic behaviour and possible interaction between the electromechanical modes, the setting of a voltage reference of slack generator was varied from 0.97 to 1.05 pu.

Dynamic behaviour of two local modes associated with damping ratio and oscillatory frequency under parameter variation is depicted in Fig. 15. Primarily, two local modes were approaching together and nearly coinciding at a frequency of 9.53 rad/s. Resonance between two local modes was identified in the range reference voltage of 1.03 to 1.04 pu, as marked by a circle. Around a resonance point, these two eigenvalues became very sensitive to parameter variation. As voltage reference of the slack generator was further varied, the two interacting modes departed oppositely. Local mode 1 moved to the left-hand side while local mode 2 shifted toward the right indicating enhancement and deterioration of system damping performance respectively.

The impact of grid-tied MG operation on modal interaction would be further analysed by connecting the hybrid MG structure in areas 1 and 2 of two area power system as depicted in Fig. 16. Increasing MG penetration in area-1 improved the damping ratio of local mode-1 considerably. While, only a small effect was experienced by local mode-2. Consequently, the distance between those two interacting modes increased proportionally. Therefore, a coupling between those two local modes became weaker. Further decrease of intense of coupling between local modes was monitored with the increase of MG penetration level. A similar result was found when the MG system was connected to area-2. Local modes 1 and 2 shifted significantly to the left-hand side of the complex plane at a higher MG penetration level. Since the distance between the two interacting modes became farther, mitigation of coupling between the two local modes was observed.

Interaction between two eigenvalues was expected when one or more similar state variables participated in both engaged modes. Contribution or participation of a particular state variable in all the interacting modes can be defined as cross participation factor (CPF). Primarily, different state variables participated in the local modes. Speed and rotor angle from G1 and G2 participated in local mode 1 while speed and rotor angle from G3 and G4 contributed in local mode 2. As those two local modes approached each other, they started to interact as indicated by CPF of particular state variables. The state variables of G1 and G2 speed and rotor angle which previously did not participate in local mode 2, started to contribute in the corresponding mode, reflecting a connection between mode 2 and mode 1. Similarly, state variables of G3 and G4 speed and rotor angle started to contribute in local mode 1, indicating a coupling of mode 1 and mode 2. The CPF values increased gradually as the interacting modes approached each other. The highest value of CPF were identified when the interacting modes were situated around the resonance point. After coinciding in a particular resonance point the intensity of modal interaction degraded proportionally as indicated by the decrease of CPF value.

The impact of increasing MG penetration on modal interaction can be monitored by evaluating the CPF values in different MG penetration levels. Figs. 17 and 18 represent the impact of connecting the hybrid MG on the CPF values when those MGs are connected to area 1 and area 2 respectively. The monitored CPF values correspond to the values when the interacting modes are approaching and leaving the resonance point. It was observed that without MG connected to the system, the two observed modes were highly connected. More contribution of the state variables from both of the engaged modes and hence higher CPF values were monitored. However, when MG was connected to the main grid, it affects the occurrence of modal interaction. A similar trend was monitored when the MG systems were connected to areas 1 and 2. As MG penetration level increased, the damping performance of the mode from area-2 was relatively unchanged. While local mode of area-1 enhanced considerably. Indeed, more significant effect on local mode 1 was monitored when the MG system was connected to area-2. As a result, with MG connected to the system, the two local modes did not approach each other as near as in the case without MG penetration. Since the distance between two interacting modes increased, only weak coupling was experienced. Increasing of power injection from the MG alleviates the intensity of coupling between these two local modes, indicated by lower values of CPF.

It was difficult to assess the strength of the modal interaction using the previous eigen-trajectories and CPF identification methods. Therefore, to quantify the coupling between eigenvalues, modal interaction index (MII) is proposed. Coupling between two interacting modes becomes stronger as two eigenvalues come

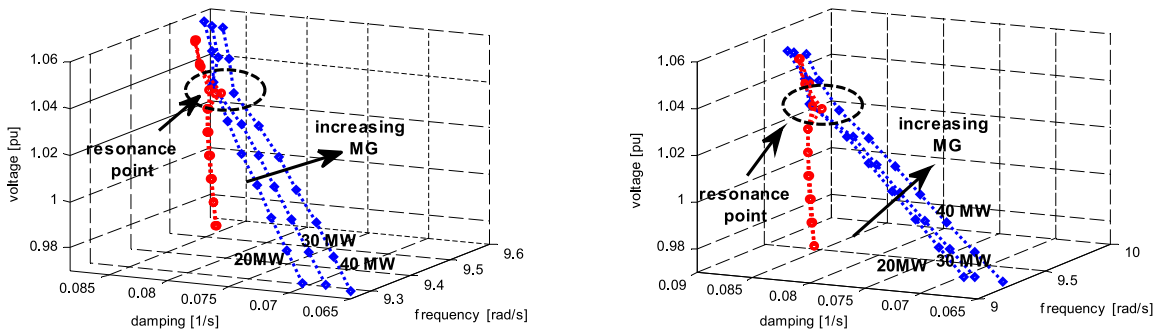

Fig. 16. Trajectories of local modes with the increasing of hybrid MG penetration in (a) area-1 and (b) area-2.

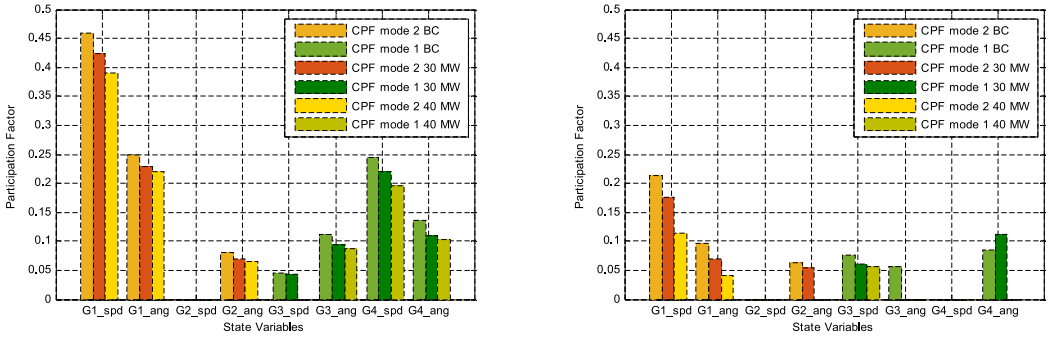

Fig. 17. CPF of interacting local modes when (a) approaching and (b) leaving the resonance point with increasing MG penetration in area-1.

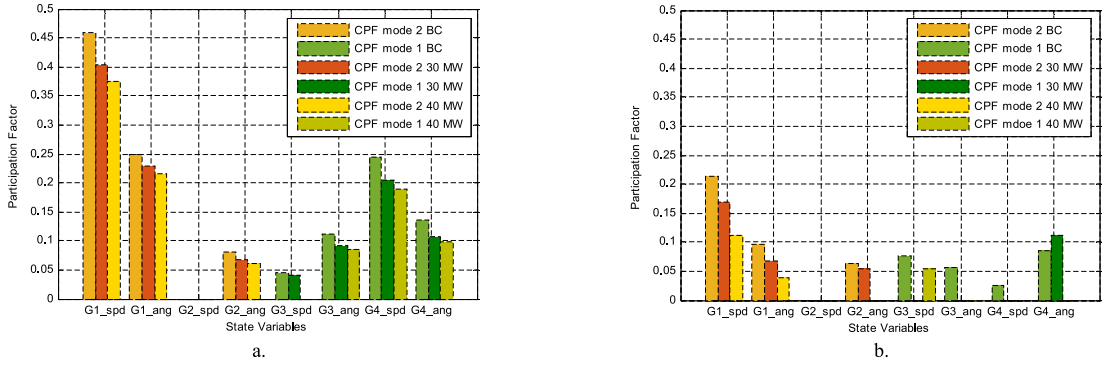

Fig. 18. CPF of interacting local modes when (a) approaching and (b) leaving the resonance point with increasing MG penetration in area-2.

closer together indicated by gradual increase of MII. The highest MII value was monitored when the engaged modes aligned in at a certain resonance point. Further variation of system parameter results in significant deviation of the interacting modes, reflected in decreasing of the MII values.

The calculated MII values under parameter variation and increasing hybrid MG penetration are depicted in Fig. 19. It was monitored that the closest distance around a resonance point was approached when generator voltage reference was set at 1.03 pu, indicated by highest MII value. In base case scenario without MG penetration, the investigated modes interacted more intensively, represented by a higher MII value. MG integration influenced the occurrence of modal interaction. As power injection from the corresponding MG systems was increased, further decrease of the MII value was monitored. Therefore, it can be considered that mitigation of modal analysis is expected at higher MG penetration levels. Compared with the impact of increasing MG penetration level when it was connected in area 1, more mitigation on modal interaction was observed when MGs were connected in area 2. Lower MII values were monitored when power injection from MG in area 2 was gradually increased.

5.3. Novel interaction between inter-area modes of power system and control modes of MG

It was obvious that grid-tied MG operation contributes to enhance system dynamic response and mitigate or even prevent the occurrence of modal interaction. Nevertheless, a sophisticated control algorithm of each DG unit in a MG introduces novel critical modes to a power system. Eigenvalues analysis observed that control modes in a MG are characterized by a low oscillatory frequency within the range of 0.1 to 0.7 Hz. This frequency region is relatively similar to the frequency range of inter-area modes. Therefore, in a certain circumstance, control modes of MG potentially interact with inter-area modes of a power system and influence the power system stability.

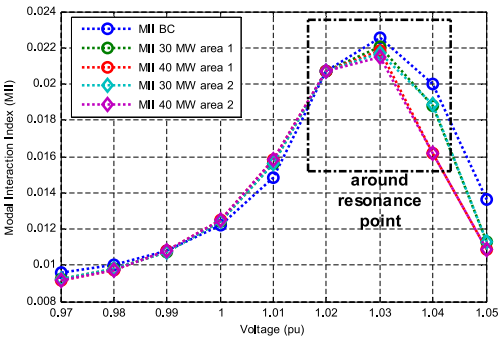

Fig. 19. MII values under increasing MG penetration.

Table 4 represents the inter-area modes in two area power system and MG control modes when the 25 MW hybrid MG was integrated. Two different RE based DG units (WECS and PV) were considered in the investigated hybrid MG system. State variables of WECS and PV based DG units participated in two different control modes. From the presented table, it can clearly be seen that the frequency range of control modes from the MG was relatively similar with oscillatory frequency of inter-area mode. Coupling between inter-area modes of a power system and control modes of each DG unit in MG is then observed by increasing power injection from the MGs from 5 to 50 MW.

Trajectories of the interacting modes and MII values in different MG penetration levels in area-1 and area-2 are depicted in Figs. 20 and 21 respectively. A more complex interaction between critical mode from MG and electro-mechanical mode of a power system might emerge under grid-tied MG operation. Coupling between three different modes corresponding to inter-area, WECS and PV control modes was monitored. At lower power injection

Table 4
Inter-area and MG control modes in two-area power system.

Investigated modes	Re.	Im.	f (Hz)
Inter-area mode	−0.0317	±3.6167	0.575
Control modes from WECS based DG unit in MG	−0.5081	±4.2094	0.672
Control modes from PV based DG unit in MG	−0.0338	±2.3094	0.368

from the MG, low oscillatory frequency mode corresponding to PV control state variables did not appear, only inter-area mode and control mode from WECS based DG unit interacted. Those two modes started to interact and approached a resonance point at 20 MW MG penetration level, indicated by the closest distance between the engaged mode and the first peak of MII values. After resonance, those two interacting modes slightly deviated. Consequently, coupling between inter-area and WECS control mode decreased proportionally, indicated by a significant decrease of MII values. As power injection from MG was further increased, control mode from PV based DG unit emerged and joined the interaction. From 25 MW MG penetration level, three modes started to interact, the monitored MII values increased gradually as the interaction among three engaged modes became more intense. However, in a specified range between 25 MW to 50 MW the second resonance point was not approached.

6. Conclusions

The impact of grid-tied MG operation on small signal stability and modal interaction considering RE uncertainties is thoroughly examined in this work. Under wind speed and solar irradiance uncertainties, local and inter-area modes of power system behaved unpredictably. When the hybrid MG was connected into area-1, more fluctuations of local modes from area-1 than local modes from area-2 and inter-area modes were observed, indicated by

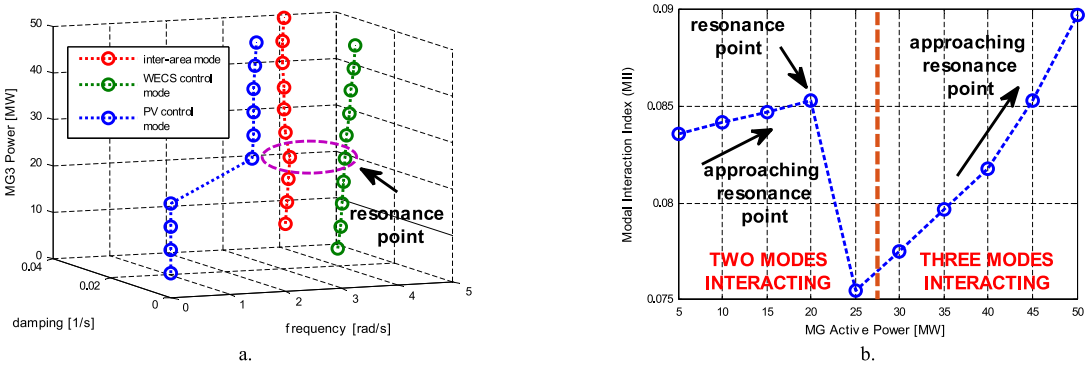

Fig. 20. Trajectories and (b) MII of the interaction between inter-area and MG control modes when the MG was connected to area-1.

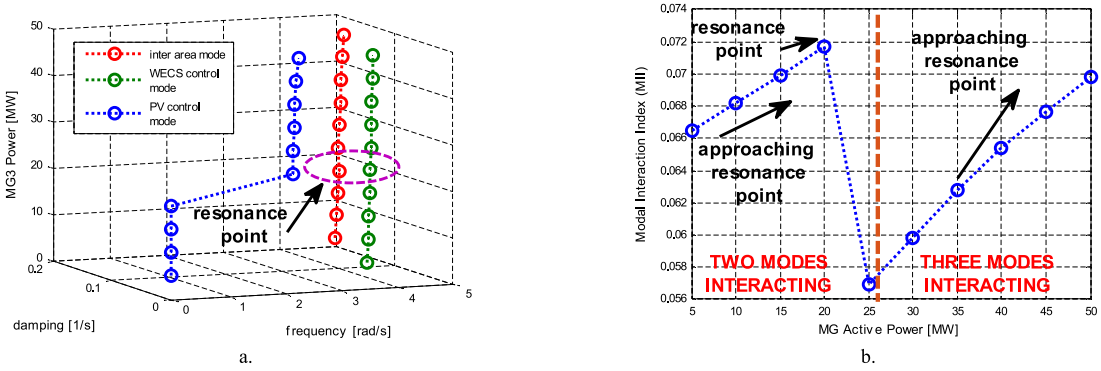

Fig. 21. (a) Trajectories and (b) MII of the interaction between inter-area and MG control modes when the MG was connected to area-2.

higher standard deviations of local mode 1 than those two critical modes. Conversely, when the MG was connected to area-2, more fluctuations of local mode 2 and inter-area modes than local mode 1 were monitored. In general, the damping ratio of critical modes enhanced variously when the grid-tied MG operations and RE uncertainties were considered. The cumulative distribution of damping ratio of critical modes improved proportionally at higher wind speed and solar irradiance profiles which resulted in higher power injections from the MG.

The research further investigated interactions between local modes due to variation of generator reference voltage. Three analytical methods i.e. eigen-trajectories, cross participation factor and modal interaction index (MII) are proposed to confirm and characterize the modal interaction. Furthermore, it is emphasized that MG influences the occurrence of modal interaction. It is clearly observed that increasing MG penetration level resulted in mitigation of interaction between local modes of power system. However, a novel interaction between inter-area modes and MG control modes possibly occurred at higher MG penetration level. In order to make sure a stable operation of power system with uncertain power injection from RE based power generation and MG, it is important to identify the occurrence of modal interaction in specific the interaction among critical modes of power system and between inter-area and control modes of MG.

Declaration of competing interest

The authors declare that they have no known competing financial interests or personal relationships that could have appeared to influence the work reported in this paper.

Acknowledgment

The Authors is very grateful to Ministry of Education, Culture, Research and Technology Indonesia for funding this research.

References

[1] Zaheeruddin, M. Manas, Renewable energy management through microgrid central controller design: An approach to integrate solar, wind and biomass with battery, in: Energy Reports, vol. 1, Elsevier, 2015, pp. 156–163.
[2] I. Dobson, Strong resonance effects in normal form analysis and subsynchronous resonance, in: Bulk Power System Dynamic and Control V. Onomichi, Japan, 2001.
[3] A.U. Krismanto, M. Nadarajah, O. Krause, Influence of renewable energy based microgrid on low frequency oscillation of power systems, in: Asia Pacific Power Energy Engineering Conference, IEEE, Brisbane, QLD, 2015.
[4] D. Gautam, V. Vittal, T. harbour, Impact of increased penetration of DFIG-based wind turbine generators on transient and small signal stability of power systems, IEEE Trans. Power Syst. 24 (3) (2009) 1426–1434.
[5] S. Lamichhane, N. Mithulananthan, Influence of wind energy integration on low frequency oscillatory instability of power system, in: Australasian Universities Power Engineering Conference, AUPEC, Perth, 2014.
[6] M. Singh, A.J. Allen, F. Eduard Muljadi, V. Gevorgian, Y. Zhang, S. Santoso, Interarea oscillation damping controls for wind power plants, IEEE Trans. Sustain. Energy 6 (3) (2015) 967–975.
[7] H.U. Banna, A. Luna, S. ying, H. Ghorbani, P. Rodriguez, Impacts of wind energy in-feed on power system small signal stability, in: 3rd International Conference on Renewable Energy Research and Application, IEEE, Milwaukee, WI, 2014, pp. 615–622.
[8] S. Dahal, N. Mithulananthan, T. Saha, Investigation of small signal stability of a renewable energy based electricity distribution system, in: Power and Energy Society General Meeting, IEEE, Minneapolis, 2010, pp. 1–8.
[9] W. Du, H. Wang, L. Xiao, Power system small-signal stability as affected by grid-connected photovoltaic generation, Eur. Trans. Electr. POWER 22 (5) (2011) 668–703.
[10] H. Liu, L. Jin, D. Le, A.A. Chowdhury, Impact of high penetration of solar photovoltaic generation on power system small signal stability, in: 2010 International Conference on Power System Technology, 2010, pp. 1–7.
[11] J.V. Milanović, Probabilistic stability analysis: the way forward for stability analysis of sustainable power systems, Phil. Trans. R. Soc. A 375 (2017) 20160296.
[12] J.L. Rueda, D.G. Colomé, I. Erlich, Assessment and enhancement of small signal stability considering uncertainties, IEEE Trans. Power Syst. 24 (1) (2009).
[13] H. Huang, C.Y. Chung, K.W. Chan, H. Chen, Quasi-Monte Carlo based probabilistic small signal stability analysis for power systems with plug-in electric vehicle and wind power integration, IEEE Trans. Power Syst. 28 (3) (2013) 3335–3343.
[14] S.Q. Bu, W. Du, H.F. Wang, Z. Chen, L.Y. Xiao, H.F. Li, Probabilistic analysis of small-signal stability of large-scale power systems as affected by penetration of wind generation, IEEE Trans. Power Syst. 27 (2) (2012) 762–770.
[15] I. Dobson, E. Barocio, Perturbations of weakly resonant power system electromechanical modes, IEEE Trans. Power Syst. 20 (1) (2005) 330–337.
[16] I. Dobson, J. Zhang, S. Greene, H. Engdahl, P.W. Sauer, Is strong modal resonance a precursor to power system oscillations? IEEE Trans. Circuit Syst. Fundam. Theory Appl. 48 (3) (2001) 340–349.
[17] A.U. Krismanto, M. Nadarajah, Identification of modal interaction and small signal stability in autonomous microgrid operation, IET Gen. Transm. Distrib. (2017).
[18] A.M. Bouzid, J.M. Guerrero, A. Cheriti, M. Bouhamida, P. Sicard, M. Benghanem, A survey on control of electroc power distributed generation system for microgrid application, Renew. Sustain. Energy Rev. 44 (2015) 751–766.
[19] J. Selvaraj, N.A. Rahim, Multilevel inverter for grid-connected PV system employing digital PI controller, IEEE Trans. Ind. Electron. 56 (1) (2009) 149–158.
[20] J.M.E. Huerta, J. Castelló-Moreno, J.R. Fischer, R. García-Gil, A synchronous reference frame robust predictive current control for three-phase grid-connected inverters, IEEE Trans. Ind. Electron. 57 (3) (2010) 954–962.
[21] S. Alepuz, et al., Control strategies based on symmetrical components for grid-connected converters under voltage dips, IEEE Trans. Ind. Electron. 56 (6) (2009) 2162–2173.
[22] I.J. Balaguer, S.Y. Qin Lei, U. Supatti, F.Z. Peng, Control for grid-connected and intentional islanding operations of distributed power generation, IEEE Trans. Ind. Electron. 58 (1) (2011) 147–157.
[23] D.E. Olivares, et al., Trends in microgrid control, IEEE Trans. Smart Grid 5 (4) (2014) 1905–1919.
[24] J. Rocaber, A. Luna, F. Blaabjerg, P.R. ıguez, Control of power converters in AC microgrids, IEEE Trans. Power Electron. 27 (11) (2012) 4734–4749.
[25] Y.T. Tan, D.S. Kirschen, N. Jenkins, A model of PV generation suitable for stability analysis, IEEE Trans. Energy Convers. 19 (4) (2004) 748–755.
[26] Y.M. Atwa, Distribution System Planning and Reliability Assessment under High DG Penetration, University of Waterloo, Ontario, Canada, 2010.
[27] S. Liu, P.X. Liu, XiaoyuWang, Stochastic small-signal stability analysis of grid-connected photovoltaic systems, IEEE Trans. Ind. Electron. 63 (2) (2016) 1027–1038.
[28] H.R. Baghaee, M. Mirsalim, G.B. Gharehpetian, H.A. Talebi, Fuzzy unscented transform for uncertainty quantification of correlated wind/PV microgrids: possibilistic–probabilistic power flow based on RBFNNs, IET Renew. Power Gener. 11 (6) (2016) 867–877.
[29] J. Park, W. Liang, J. Choi, A.A. El-Keib, M. Shahidehpour, R. Billinton, A probabilistic reliability evaluation of a power system including solar/photovoltaic cell generator, in: Power & Energy Society General Meeting, 2009. PES '09, IEEE, Calgary, AB, Canada, 2009.
[30] R.-H. Liang, J.-H. Liao, A fuzzy-optimization approach for generation SchedulingWithWind and solar energy systems, IEEE Trans. Power Syst. 22 (4) (2007) 1665–1674.
[31] W. Zhou, C. Lou, Z. Li, L. Lu, H. Yang, Current status of research on optimum sizing of stand-alone hybrid solar–wind power generation systems, Appl. Energy 87 (2010) 380–389.
[32] J. Hetzer, D.C. Yu, K. Bhattarai, An economic dispatch model incorporating wind power, IEEE Trans. Energy Convers. 23 (2) (2008) 603–611.
[33] X. Liu, Optimization of a combined heat and power system with wind turbines, Electr. Power Energy Syst. 43 (2012) 1421–1426.
[34] A.U. Krismanto, N. Mithulananthan, I. Kamwa, Oscillatory stability assessment of microgrid in autonomous operation with uncertainties, IET Renew. Power Gener. 12 (4) (2018) 494–504.
[35] P. Kundur, N.J. Balu, M.G. Lauby, Power System Stability and Control, McGraw-Hill, New York, NY, USA, 1994.
[36] M.K. Zadeh, M. Amin, J.A. Suul, M. Molinas, O.B. Fosso, Small-Signal Stability Study of the Cigré DC Grid Test System with Analysis of Participation Factors and Parameter Sensitivity of Oscillatory Modes, Power Systems Computation Conference (PSCC). Power Systems Computation Conference, 2014.
[37] K.R. Padiyar, Analyis of Subsynchronous Resonance in Power System, Springer Science, New York, 1999.
[38] J. Beerten, S. D'Arco, J.A. Suul, Identification and small-signal analysis of interaction modes in VSCMTDC systems, IEEE Trans. Power Deliv. 31 (2) (2016).